Catalysis Today 175 (2011) 362–369

Contents lists available at ScienceDirect

Catalysis Today

journal homepage: www.elsevier.com/locate/cattod

Trinuclear iron cluster intercalated montmorillonite catalyst: Microstructure and photo-Fenton performance

Shilong Zhang, Shijing Liang, Xiaowei Wang, Jinlin Long, Zhaohui Li, Ling Wu*

State Key Laboratory Breeding Base of Photocatalysis, Research Institute of Photocatalysis, Fuzhou University, Fuzhou 35002, PR China

ARTICLE INFO

Article history:
Received 31 October 2010
Received in revised form 15 February 2011
Accepted 28 February 2011
Available online 9 April 2011

Keywords:
Photo-Fenton
Iron cluster
Montmorillonite
Phenol degradation

ABSTRACT

Trinuclear Fe (III) acetato complex intercalated montmorillonite Fenton catalysts with large surface areas were prepared by a facile ion exchange process. The obtained samples were characterized by FT-IR, TGA-DSC, N_2-sorption and XPS in detail. To understand the microstructure of the active iron species in the montmorillonite, the Fe K-edge X-ray absorption spectra (XAFS) technique was also employed. The results showed that the trinuclear iron cluster was successfully intercalated into the layers of montmorillonite and the structure of the active iron species was an amorphous FeO(OH)-like structure after 500 °C post-treatment. When the prepared catalysts were used for the photo-Fenton reaction at room temperature, excellent activities were observed for degradation of phenol. Moreover, their activities were much higher than those of the traditional iron hydroxyl compound intercalated montmoillonite Fenton catalyst. The stable intercalated structure and the low leaching Fe concentration induced that the obtained catalyst can be operated for a long time. Meanwhile, the consumption of H_2O_2 and the change of pH in solution were also investigated in detail.

1. Introduction

Heterogeneous photo-Fenton reaction has attracted tremendous attention as one of the most important advanced oxidation techniques in wastewater treatment. Its unique advantages can be briefly expressed as follows: (1) quick and sufficient mineralization of toxic and refractory contaminants, (2) long operation life and reaction can be performed at a wide range of pH values, (3) facile recovery and easy separation of the heterogeneous catalysts from the treated wastewater. Among various heterogeneous photo-Fenton catalysts, iron ions, iron clusters, and Fe oxides mainly act as active species for photo-Fenton reaction. For the reasons of low surface area of iron oxides and the iron ion leakage problem, amounts of researches target to loading the Fe complex on various supports, such as zeolites [1,2], resin [3], clays [4,5] and nafion membranes [6].

Montmorillonite, one of the layered aluminosilicate minerals, is widely known support owing to its low cost and its unique physicochemical properties. Both the cation exchange capability and negative charge of the montmorillonite make it suitable for embedding ionic nanoparticles *via* an exchange method. Some metal oxides [7–10] and organic polycompounds [11–13] were introduced to prepare the modified montmorillonite which owns special properties. Extensive studies have focused on the Fenton catalysts which utilize the iron hydroxyl, and iron ions as iron source to intercalate into the montmorillonite [14–20]. Although the surface area of the catalysts prepared by this method can be obviously enhanced, these inorganic iron compounds of intercalated montmorillonite suffered from the limitation of thermal stability [21]. Their intercalated structures were easily collapsed during the post-treatment. According to the previous reports [13,15,22], the specific surface area and the micropore volume of the catalyst would be increased remarkably if a large iron cluster or compound is intercalated into the layers of montmorillonite, that is more catalytic sites are provided by the modified montmorillonite catalyst. Thus, the activities of the catalysts can be increased higher and higher by intercalating larger iron clusters.

The structure of trinuclear iron acetato cluster consists of a regular triangular Fe_3O unit with the iron octahedrons which are connected by bridging six acetate groups. Yamanaka et al. reported this trinuclear iron cluster can be intercalated into the layers of montmorillonite [23]. For the large diameter and a relatively stable structure of this compound, the intercalated montmorillonite exhibited a large surface area and retain the intercalated structure even under the calcination of 500 °C. However, this promising compound's photo-Fenton activities have not been investigated in detail. Moreover, iron species exist in various forms in the montmorillonite [24–26], even are calcined under a high temperature. And the chemical properties are highly correlated with the composition and the chemical environment. So it would be interesting to study on the Fenton performance of the catalyst and the microstructure of the active iron species in the montmorillonite.

* Corresponding author. Tel.: +86 591 8377 9362; fax: +86 591 8377 9105.
E-mail address: wuling@fzu.edu.cn (L. Wu).

0920-5861/$ – see front matter © 2011 Elsevier B.V. All rights reserved.
doi:10.1016/j.cattod.2011.02.054

Herein, a large trinuclear iron cluster was intercalated into the layers of commercial montmorillonite by a facile cation exchange method. The chemical environments and structures of the active iron species in the montmorillonite have been determined by XAFS and XPS techniques. The photo-Fenton performances of the catalysts were evaluated by degradation and mineralization of phenol solution. Meanwhile, the as-prepared catalysts may be used as good candidates for photo-Fenton reaction compared with the traditional iron hydroxyl cation intercalated montmorillonite (IHCIM) catalyst. Furthermore, to understand the essence of the prepared catalysts with high photo-Fenton activities, some influence factors, such as the decomposition of H_2O_2, the leaching iron concentration and the change of pH value in solution, were investigated in detail.

2. Experimental

2.1. Chemical and materials

Commercial Montmorillonite K10, with a cationic exchange capacity (CEC) of 83 mequiv./100 g of clay was purchased from J&K chemical Co. Iron nitrate ($Fe(NO_3)_3{\cdot}9H_2O$), sodium acetate ($CH_3COONa{\cdot}3H_2O$), sulfuric acid (H_2SO_4), phenol and hydrogen peroxide H_2O_2 (30% aqueous solution) were obtained from Sinopharm Chemical reagent Co., Ltd. (Shanghai, China). All chemicals were of analytical grade reagents without further purification.

2.2. Preparation of iron precursor intercalated montmorillonite

The intercalated montmorillonite was prepared by a typical cation exchange method. Firstly, the trinuclear Fe (III) acetato complex ($[Fe_3O(COOCH_3)_3{\cdot}3H_2O]_6{\cdot}NO_3$, denoted as Fe_3O) was prepared by a modified method: 20 g $CH_3COONa{\cdot}3H_2O$ and 29.7 g $Fe(NO_3)_3{\cdot}9H_2O$ were dissolved in 50 mL H_2O. The reacting system was refluxed under 70 °C for 8 h. Then the solution was transferred to a sealed container which fitted with a certain volume of sulfuric acid. After several days, lots of large crystals were grown under the container. The products were filtered and washed, and then the polycation iron cluster compound was obtained. After that, 8 mmol polycation iron compound was dissolved in 100 mL deionized water under a vigorous stirring at room temperature. 4 g commercial montmorillonite treated by Na_2CO_3 was added into the obtained polycation iron solution. The iron complex intercalated montmorillonite sample was centrifuged and washed with deionized water after stirring for 48 h. This intercalated clay was dried at 80 °C and denoted as Fe_3O-K10. In addition, the Fe_3O-K10 was calcined and activated at 500 °C, the obtained sample was denoted as Fe_3O-K10-500. Meanwhile, the traditional IHCIM catalyst was prepared as per the previous report [15] and used for a comparison of photo-Fenton activities.

2.3. Characterization of catalyst

Fourier transform infrared spectra (FT-IR) were obtained with a Nicolet 670 FT-IR spectrometer to monitor the sequential change of the chemical species. The thermal stability analysis (TGA/DSC) was carried out on a TG-DSC STA 449C Jupiter analyzer with an air purging gas, at a heating rate of 5 °C min^{-1} from 30 to 700 °C. The specific surface areas of the samples were measured by N_2-sorption at 77 K on Micromeritics ASAP 2020 analyzer and calculated by the Brunauer–Emmett–Teller (BET) method. X-ray photoelectron spectroscopy (XPS) measurements were performed on an ESCALAB 250 photoelectron spectroscopy (Thermo Fisher Scientific) at 3.0×10^{-10} mbar with monochromatic Al Kα radiation (E = 1486.2 eV). X-ray absorption spectra (Fe K-edge at 7.112 keV) were measured at the XAFS station (Beam line BL14W1) of the Shanghai synchrotron Irradiation Facility (SSRF) with stored electron energy of 3.5 GeV and ring currents of 200 mA. Data were collected in a fluorescence mode at room temperature. And the data treatments were carried out by using the software package WinXAS2.0.

2.4. Activity measurements

The photo-Fenton activities of the samples were evaluated by the decomposition of phenol in aqueous solution. The concentration of the freshly prepared phenol solution was 8.0×10^{-4} M. A typical experiment was performed in a 200 mL quartz reactor (150 mg catalyst, 150 mL phenol solution) surrounded by three UV lamps (Philips, TUV 4W/G4 T5, 254 nm). Prior to irradiation, the suspension was continuously stirred till an adsorption/desorption equilibrium of the phenol was established on the catalysts. Then the given concentration of H_2O_2 aqueous solution was added into the suspensions before the radiation. The initial pH of the solution was pH 6.0 and the temperatures of reaction system were kept at 20 ± 2 °C. At given irradiation time intervals, 10 mL of the suspension was collected and centrifuged to remove the catalyst at once, and the concentrations of phenol and H_2O_2 [27] were analyzed with a UV–vis spectrophotometer (Varian Cary 50). The mineralization of phenol solution was detected by the total organic carbon by a Shimadzu TOC-V (CPH) total carbon analyzer.

3. Results and discussion

3.1. Characterization of Fe_3O/montmorillonite samples

Fig. 1 shows that curve a is the spectrum of Na-form montmorillonite, the strong absorption band at 1067 cm^{-1} is the uniquely characteristic vibration of Si–O and Si–O–Si in the clay lattice. The peak at 3430 cm^{-1} is assigned to the contribution of the clay lattice and surface absorbed –OH stretching vibrations. After the iron precursor is intercalated into the montmorillonite, curve b exhibits two special peaks at 1592 cm^{-1} and 1448 cm^{-1}, corresponding to the symmetric and as-symmetric vibrations of the carboxylate groups (COO^-) of the trinuclear Fe (III) acetato complex, respectively. These results are very similar to those of the previous report [23] and it suggests that the iron species is a trinuclear Fe (III) acetato complex. However, when the sample was calcined at 500 °C, as shown in curve c, the characteristic peaks of carboxylate groups

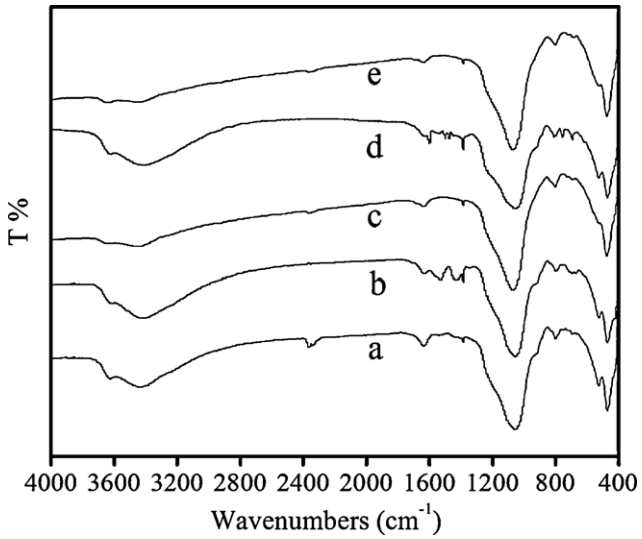

Fig. 1. FT-IR spectra of (a) Na-K10, (b) Fe_3O-K10, (c) Fe_3O-K10-500, (d) Fe_3O-K10-500 absorbed phenol, and (e) Fe_3O-K10-500-phenol sample after Fenton reaction.

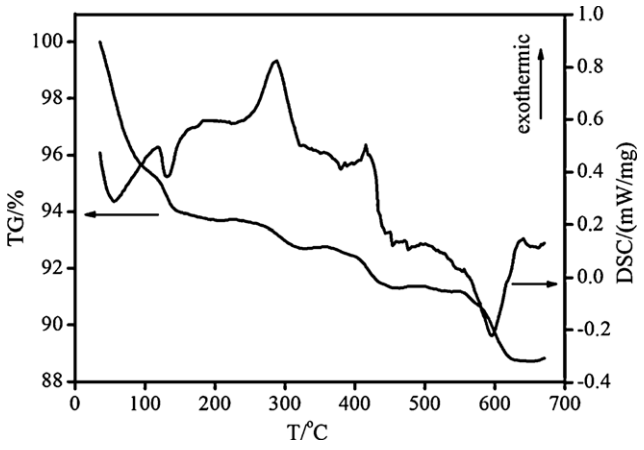

Fig. 2. TGA/DSC curves of the Fe_3O-K10 sample tested in air at temperature raising rate of 5 °C min^{-1}.

diminished because the iron cluster has decomposed into other composition. The peak intensities of –OH stretching vibrations are lower than those of curves a and b. By absorbing the phenol solution on the catalyst, we find some characteristic peaks of the phenol and intermediates at (1370–1650 cm^{-1}). The peaks at 1600, 1500 and 1472 cm^{-1} are assigned to the ring breathing vibration of the benzene, while the peak at 1380 cm^{-1} is contributed to the C–H bending vibration. All these peaks disappeared when the photo-Fenton reaction completed (curve e), it indicated that the phenol and intermediates have been easily absorbed on the catalyst and fully mineralized into CO_2 and H_2O.

The thermal transformation of the Fe_3O-K10 sample was studied by TGA/DSC in air up to 700 °C. As shown in Fig. 2, four losses of weight can be observed from the TGA curves. The weight loss occurs from 50 to 150 °C and amounts to 6.40%, which can be attributed to the loss of physically adsorbed water molecule on the surface of the iron montmorillonite. The endothermic peaks at 55 °C and 130 °C in the DSC curve confirm this contribution. The next step mass change occurs between 240 and 300 °C, and the obvious exothermic peak of the DSC curve at 286 °C indicates that the carboxylate ligands are decomposed at this temperature region [4]. The third mass loss, taking place at a temperature range of 400–600 °C and accounting for a weight loss about 3.54%, is due to the loss of water molecules that are hydrogen-bonded to the interlayer of montmorillonite. A sharp weight decrease and a wide endothermic peak can be observed from the TGA curve and the DSC curve, respectively; it indicates a full dehydroxylation [26] at this temperature region.

The BET surface areas of the Na-K10, Fe_3O-K10 and Fe_3O-K10-500 samples are shown in Table 1. The Na formed montmorillonite exhibits a surface area of 188.6 m^2/g. While the montmorillonite surface area is greatly enlarged after the iron cluster intercalated into the two layers of SiO_4 tetrahedrons, the value of BET surface area reaches to 281.4 m^2/g. In addition, the value of 500 °C treatment sample's surface area is 258.8 m^2/g, which is slightly smaller than that of the Fe_3O-K10 sample. Moreover, the external and internal surface has been evaluated by t-plot method. Both dates indicate that the external surface areas of iron intercalated samples are enlarged compared with the Na-montmorillonite. The adsorption–desorption isotherms of all samples are a type IV

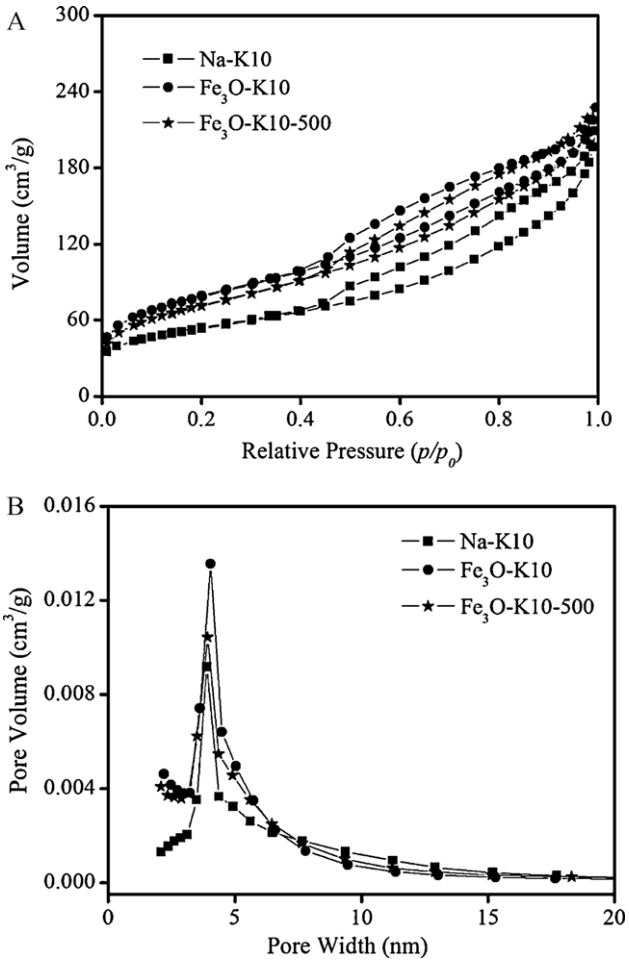

Fig. 3. The typical N_2 adsorption–desorption isotherm (A) and corresponding pore diameter distribution (B) of the Na-K10, Fe_3O-K10, and Fe_3O-K10-500 samples.

isotherm with a hysteresis loop (Fig. 3A). As shown in Fig. 3B, the most probable values of samples' pore size are about 4 nm.

The XPS spectra were recorded to study the surface chemical states of the obtained samples. The survey spectra of the iron cluster intercalated montmorillonite samples are similar, which mainly contain the Fe, Si, Al, O and C elements (Fig. 4A). The C1s spectrum of the Fe_3O-K10 sample is different from the other two samples, as shown in Fig. 4(B), besides the strong peaks at 284.6 eV assigned to adventitious elemental carbon, there are another two peaks at 286.4 and 288.4 eV, which can be ascribed to carbon from Fe_3O. For the O1s spectrum (Fig. 4C), two peaks separately at 532.25 and 531.25 eV indicate the lattice oxygen in the montmorillonite and surface absorbed hydroxyl groups in the three samples, while another peak at 530.1 eV in the iron intercalated samples may be attributed to oxygen from Fe_3O. The high resolution spectra of iron element (Fig. 4D) show that the core lines were fixed at 711.1 eV (Fe $2p_{3/2}$) and 724.75 eV (Fe $2p_{1/2}$), which are in good agreement with the previous report [28]. The differences still can be observed in the Si 2p (Fig. 4E) and Al 2p (Fig. 4F) spectra, both the results show the chemical states have changed in three samples. The above

Table 1
Textural characteristic of the Na-K10, Fe_3O-K10, Fe_3O-K10-500 samples.

Samples	BET surface area (m^2/g)	External surface area (m^2/g)	Internal surface Area (m^2/g)	Fe content (w/w, %)
Na-K10	188.6	150.3	38.3	0.27
Fe_3O-K10	281.4	242.4	39.0	6.78
Fe_3O-K10-500	258.8	236.0	22.8	7.57

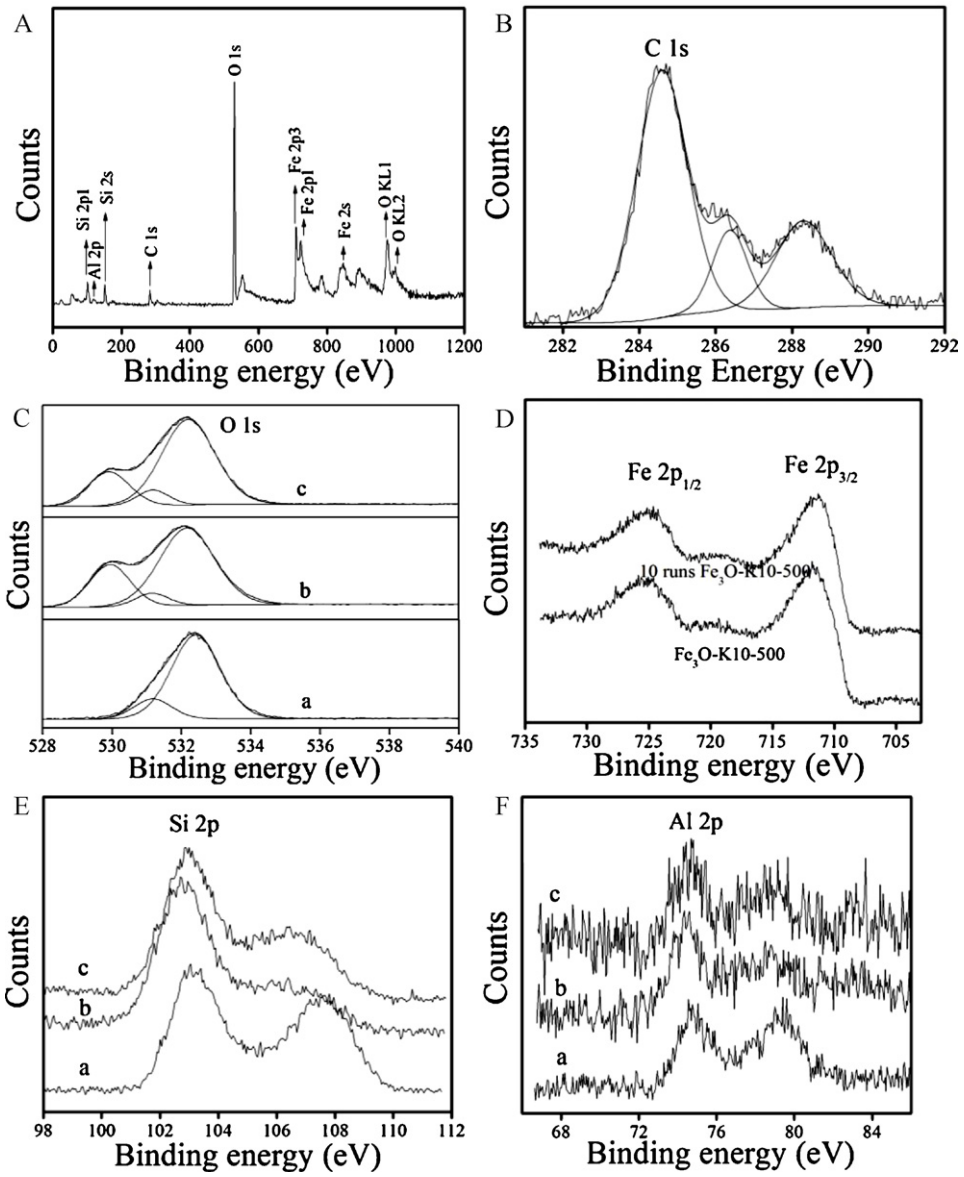

Fig. 4. The XPS spectra of surface elements of the samples (A) survey spectra, (B) C element, (C) O element, (D) Fe element, (E) Si element, and (F) Al element; (a) Na-K10, (b) Fe_3O-K10, and (c) Fe_3O-K10-500.

XPS results also suggest that the trinuclear Fe acetato complex has effectively intercalated into the montmorillonite.

3.2. Determination of the iron species

The iron species of traditional iron hydroxyl intercalated Fenton catalyst has been determined as α-Fe_2O_3 as reported by Feng [15,16]. What about the Fe_3O intercalated montmorillonite? Is it also similar to the traditional Fenton catalyst? So, we utilize the XAFS technique to determine the active iron species in the as-prepared samples. Fig. 5A shows the normalized Fe–K edge XANES spectra of the prepared samples with α-Fe_2O_3 as a standard reference. The edge positions and features of the listed samples matched well with the reference α-Fe_2O_3, indicating that the valent state of iron element is the trivalent state in these samples. The pre-edge absorption in Fe K-edge XANES spectra originates from a 1s–3d transition, which is forbidden in strictly octahedral coordination but is allowed in coordination without inversion center [29]. As shown in Fig. 5B, the Fe_3O showed the lowest pre-edge peak intensity, which is due to iron located in an almost ideal octahedron, while the lower pre-edge peak intensity than that of α-Fe_2O_3 also indicates a more centrosymmetric iron coordination environment than the reference α-Fe_2O_3 (distorted octahedral coordination [30]). Both Fe_3O-K10 and Fe_3O-K10-500 samples exhibit a more intense and narrower pre-edge than the reference α-Fe_2O_3, while the pre-edge features are lower than those of the four-coordinated iron of ferrisilicate reported in the previous study [31]. The changed features indicate a more distorted coordination environment of the iron species in the two samples. Additional, more differences between the intercalated samples and the reference α-Fe_2O_3 can also be found in the edge shape and the post-edge region. The pre-edge XANES results indicate the chemical state of the iron precursor has changed [23] but not a reduction-oxidation process.

The chemical coordination environment of iron oxide species has been determined quantitatively by performing EXAFS analysis. K^3-weighted EXAFS Fourier transformation spectra of α-Fe_2O_3 and Fe_3O-K10-500 sample are plotted in Fig. 5C, the reference Fe_2O_3 exhibits a FT peak at ~1.6 Å that originates from the Fe-O coordination shells, two peaks at 2.4–3.4 Å attribute to two kinds of Fe–O–Fe [32], another peak at ~4.0 Å due to the contribution of

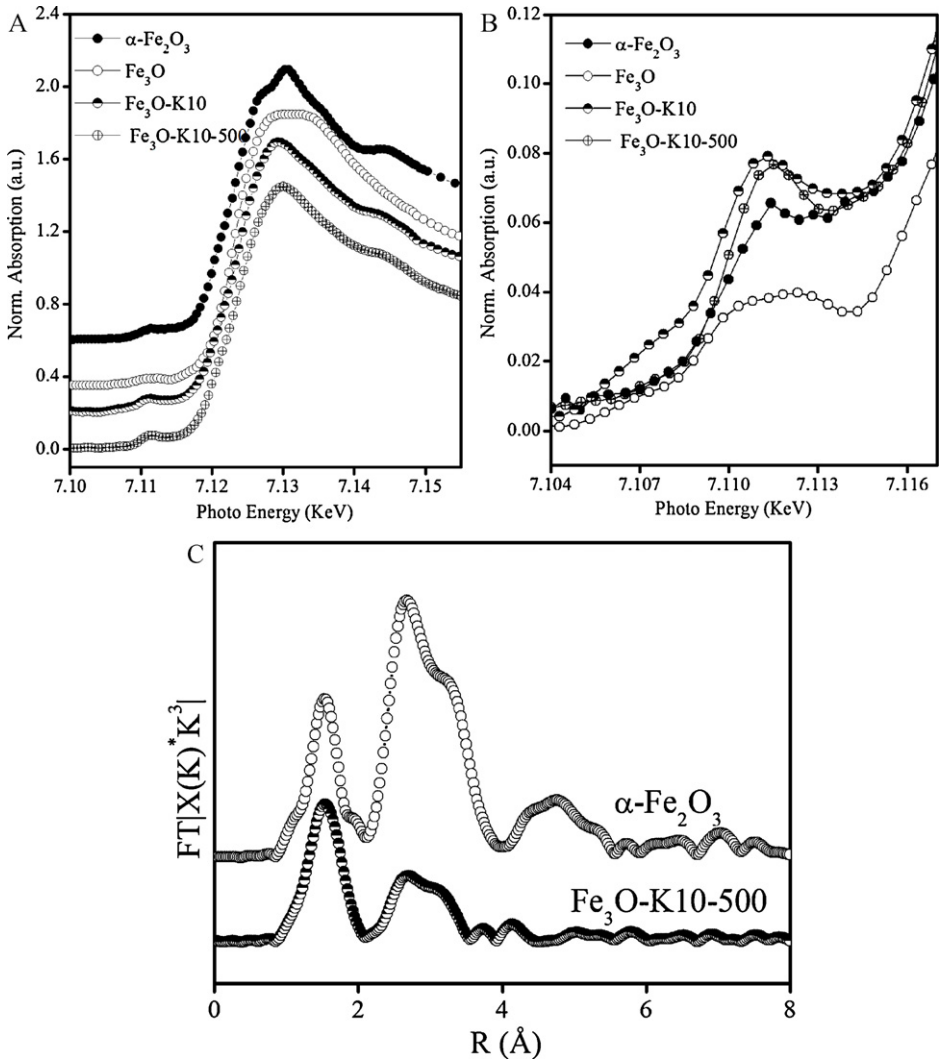

Fig. 5. The normalized Fe K-edge XANES spectra (A and B), Fourier transformations of K^3-weighted EXAFS spectra(C) for the iron intercalated samples as well as the reference compounds α-Fe_2O_3 and Fe_3O.

the large oxide particle [29]. The Fe_3O-K10-500 sample still displays several FT peaks at ~1.6 Å and 2.8 Å, but no peaks observed beyond 3.6 Å, indicating the existence of iron oxide species which are highly dispersed in the layers of montmorillonite. The peaks at ~1.6 Å still attribute to Fe–O coordination, while the peaks at 2.8 Å may become complicated for the multiple contributions of Fe–Si, Fe–Al scattering as well as Fe–Fe scattering [30]. The coordination number (CN), bond length (R), and the Debye–Waller factor (δ) are determined by the FEFF simulation, and the best fitting results of the Fourier-filtered EXAFS spectra are listed in Table 2. Upon comparison of structure parameters, it can be obviously observed that the Fe_3O-K10-500 sample more closely resembles

Table 2
The results fitting for the Fe K-edge EXAFS spectra of the Fe_3O-K10-500 sample and the reference of α-Fe_2O_3.

Sample	Shell	CN	R (Å) (10%)	δ^2 ($\times 10^{-3}$ Å^2) (10%)	ΔE_0 (eV) (10%)
α-Fe_2O_3	Fe–O	3.0	1.95	3.92	15.14
	Fe–O	3.0	2.10	7.11	9.88
	Fe–Fe	3.0	2.95	4.26	13.59
	Fe–Fe	3.0	3.35	4.36	7.04
	Fe–Fe	6.0	3.68	8.52	10.22
Fe_3O-K10-500	Fe–O	3.0	1.92	5.04	13.66
	Fe–O	3.0	2.04	6.67	11.0
	Fe–Fe	2.0	3.03	8.43	22.0
	Fe–Fe	2.0	3.42	5.64	4.36
	Fe–Fe	4.0	3.66	6.60	11.51
FeO(OH) (ICSD no. 163341)	Fe–O	3.0	1.97		
	Fe–O	3.0	2.14		
	Fe–Fe	2.0	3.02		
	Fe–Fe	2.0	3.29		
	Fe–Fe	4.0	3.44		

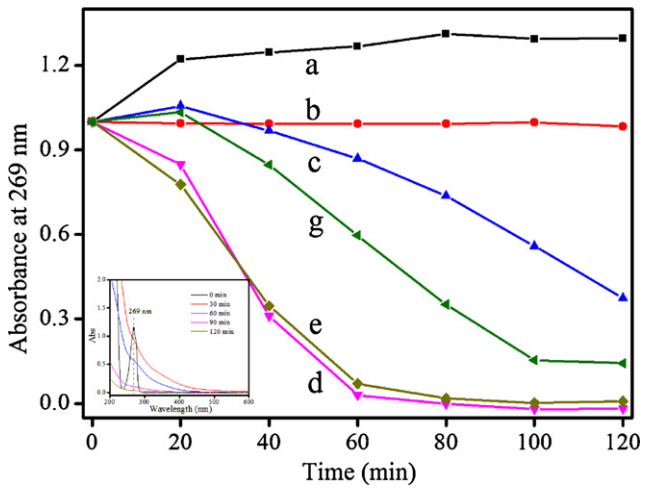

Fig. 6. Effect of various experimental conditions on degradation of phenol (8×10^{-4}M): (a) UV; (b) Fe_3O-K10-500 + H_2O_2 + dark; (c) H_2O_2 + UV; (d) $Fe(OH)_n$-500 + H_2O_2 + UV; (e) Fe_3O-K10 -500 + H_2O_2 + UV.

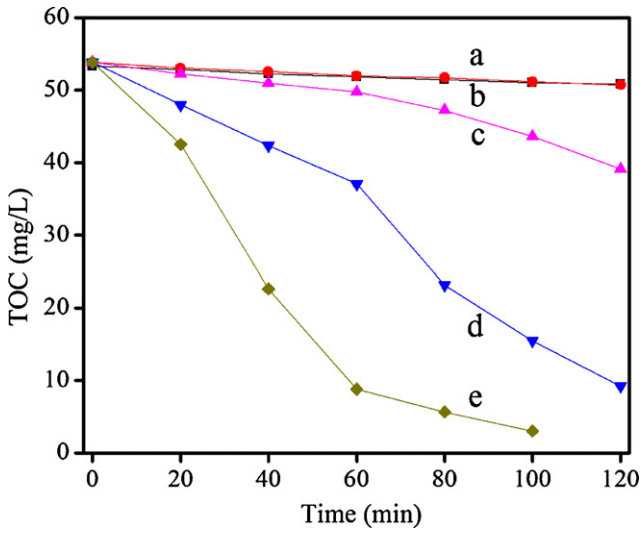

Fig. 7. Effect of various experimental conditions on mineralization of phenol (8×10^{-4} M): (a) UV; (b) Fe_3O-K10-500 + H_2O_2 + dark; (c) H_2O_2 + UV; (d) $Fe(OH)_n$-500 + H_2O_2 + UV; (e) Fe_3O-K10-500 + H_2O_2 + UV.

the parameters of FeO(OH) than those of α-Fe_2O_3 [33]. In this way, it can be concluded that the mainly iron species components in the montmorillonite should form the FeO(OH)-like amorphous clusters [34].

3.3. Photo-Fenton degradation of phenol in aqueous solution

The photo-Fenton activity of the Fe_3O-K10-500 sample was investigated in the photo-assisted degradation of phenol in the presence of H_2O_2 and UV light. Fig. 6 shows the degradation of 8×10^{-4} M phenol solution as a function of time under different experimental conditions. In this experiment, the dose of H_2O_2 and Fenton catalyst is persisted to 10 mM and 1 g/L. Curve a shows without H_2O_2 and Fe_3O-K10-500, only under the UV light radiation, the absorbance of the solution has slightly increased. It is assigned to the intermediates (resorcinol, hydroquinone, and catechol), which exhibit deeper color [35]. A negligible degradation of phenol was observed in the presence of catalyst and H_2O_2 in the darkness (curve b). This is different from the tradition Fenton reaction which can happen in the darkness, because the tradition Fenton reagents are ferrous ion (Fe^{2+}) and hydrogen dioxide. The decomposition of phenol is remarkable in the presence of H_2O_2 and UV light irradiation due to hydroxyl radical yielded (curve c). The phenol was almost degraded after 60 min in the presence of Fe_3O-K10-500, H_2O_2 and UV light irradiation (curve e). Moreover, the activity is much higher than that of the traditional IHCIM catalyst.

It is known that the degradation of phenol can form various reaction intermediates, such as benzoquinone, maleic acid, hydroquinone, and catechol, some of them may be more toxic. Hence, it was investigated that the mineralization of the phenol solution is very important to guide actual application. As shown in Fig. 7, obviously, the TOC values decrease significantly depending on various conditions. The blank experiment indicated that the phenol cannot be mineralized under UV light irradiation (Curve a). No obvious decline was observed in the presence of catalyst and H_2O_2 in the darkness (curve b). Curve c shows that the TOC removal value has been improved under both the H_2O_2 and UVC irradiation, while the TOC removal value is only 13.77 mg/L. In the presence of Fe_3O-K10-500, H_2O_2 and UV light irradiation, the TOC value of phenol solution decreases from 53.84 mg/L to 2.0 mg/L (curve e), indicating that the phenol can be fully mineralized after 100 min. Moreover, the TOC removal values of phenol *via* the homogeneous and heterogeneous Fenton reaction are 15.1 and 45.0 mg/L after 60 min under the same experimental conditions, respectively. The results indicate that the heterogeneous photo-Fenton reaction may be the main reaction in the degradation of phenol. As a comparison, the TOC value of the phenol solution over the IHCIM catalyst is still 8 mg/L after 120 min (curve d). It shows that the photo-Fenton activity of Fe_3O-K10-500 is much higher than that of the IHCIM catalyst.

In the heterogeneous photo-Fenton process, H_2O_2 is an important oxidant to provide •OH radical, which plays a key role in the heterogeneous photo-Fenton reaction [36,37]. The decomposition of H_2O_2 takes place at the same time when photo-Fenton mineralization of phenol, by detecting the residue H_2O_2 concentration can indirectly obtain the status of mineralized phenol solution. As the results presented in Fig. 8, in the dark condition (curve b), the Fe_3O-K10-500 could hardly decompose the H_2O_2 without the UV light irradiation. Then in the presence of UV light irradiation (curve c), the H_2O_2 was slowly destroyed by the UV light and about 60% H_2O_2 concentration decomposed in 120 min. It suggests that some of the H_2O_2 can be directly photolysed into •OH radical. Curve d

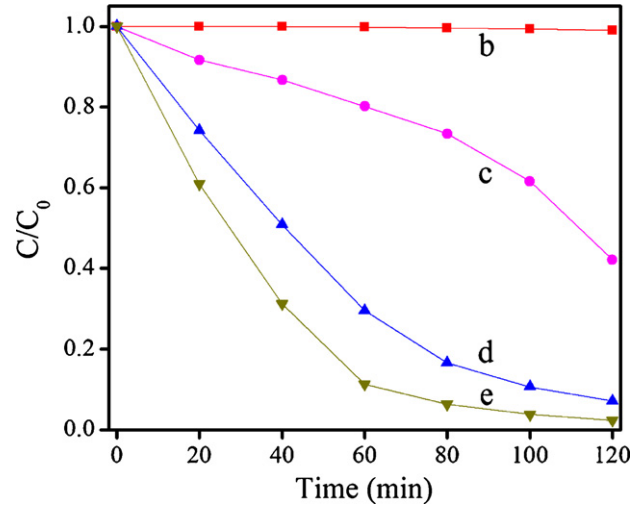

Fig. 8. Effect of various experimental conditions on decomposition of H_2O_2 (10 mM): (a) UV; (b) Fe_3O-K10-500 + H_2O_2 + dark; (c) H_2O_2 + UV; (d) $Fe(OH)_n$-500 + H_2O_2 + UV; (e) Fe_3O-K10-500 + H_2O_2 + UV.

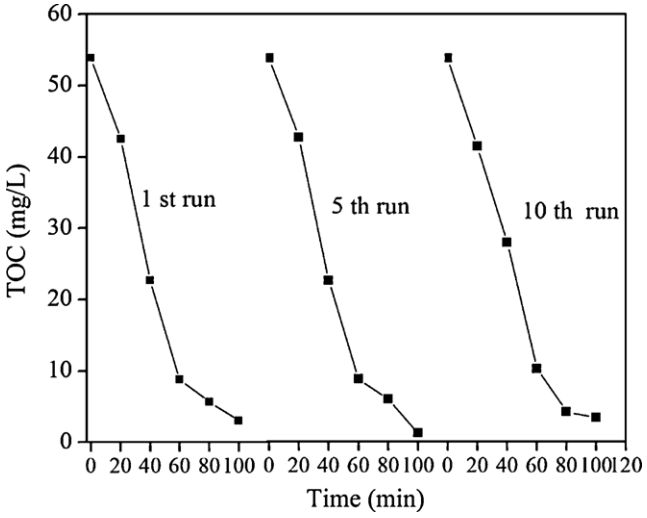

Fig. 9. Cyclic degradation of phenol as a function of time. The experimental conditions are: [Phenol] = 8×10^{-4} M/run, [H_2O_2] = 10 mM, catalyst = 1 g/L, pH 6.0.

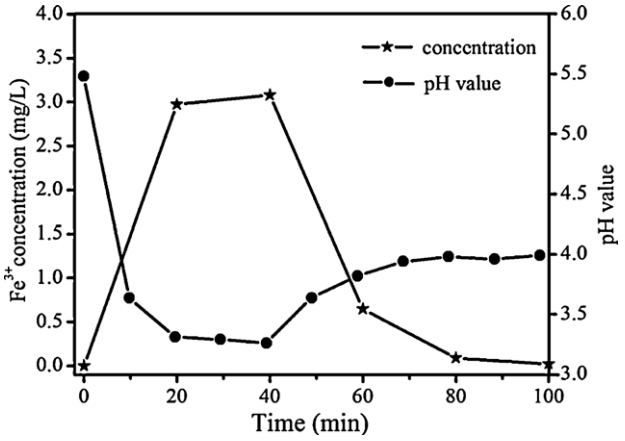

Fig. 10. Fe ion leaching concentration and pH value in the reaction solution as a function of time. The experimental condition is: [Phenol] = 8×10^{-4} M, [H_2O_2] = 10 mM, catalyst 1 g/L, pH 6.0.

shows the decomposition of H_2O_2 in the presence of Fe_3O-K10-500 and UV light irradiation. The decomposition rate of hydrogen peroxide is the best and a large amount of H_2O_2 can be decomposed in 100 min. While in the presence of the IHCIM catalyst and UV light irradiation (curve e), the rate is slower than that of Fe_3O-K10-500. These results are in good agreement with the decline of TOC value (Fig. 7).

The chemical stability is a very important feature for the catalyst when it is used in a practical industry application. The stability of the prepared catalyst was evaluated by the additional fresh phenol solution with the used catalyst from the previous run. In this procedure, the sample was reused over 10 times and its Fenton activities were evaluated by detecting the TOC decline of phenol solution. As shown in Fig. 9, the catalyst can keep catalytic activities in the multiple runs and no noticeable loss of the activity was observed during the whole reaction process. It indicates that the activity of the obtained sample is very stable. Furthermore, the surface chemical state of the recovery Fenton catalyst was examined by XPS, as shown in Fig. 3D. The result confirms that the catalyst is chemically stable in the multiple photo-Fenton runs.

Above-mentioned discussions indicate that the prepared Fenton catalyst exhibits good photo-Fenton activities both on degradation and on mineralization of phenol solution. However, there is still a problem that whether the •OH radicals come from the heterogeneous photo-Fenton reaction or from the homogeneous photo-Fenton reaction owing to the iron ion leaching problem from the catalyst. The concentration of iron ions in the suspension was detected by ICP as a function of time in this study. Additionally, the pH value in the reaction solution was also measured, aiming to interpret the iron leaching concentration in solution. As the results presented in Fig. 10, clearly, no leaching iron ions were detected in the initial solution, which has attained a dynamic absorption–desorption equilibrium. With the UV light on, the iron leaching concentration increases initially from 0 to 3 ppm and then followed by a continuous decrease. On the contrary, the pH value of the suspension changed from neutral to acid, and then gradually increased. It should be noticed that the iron ion concentration comes to a peak value of 3.08 ppm and the pH value of the solution is 3.26 after 40 min irradiation. However, the iron ion concentration is less than 0.05 ppm and pH value increases to 4.04 at the end of the reaction. The above results indicate that the iron ion leaching from the Fe_3O-K10-500 catalyst is negligible. Moreover, the solution pH value may influence the iron leaching concentration.

4. Conclusion

In conclusion, the photo-Fenton catalysts with large surface areas were successfully prepared by introducing the large trinuclear Fe (III) acetato complex intercalated into the layers of montmorillonite. The structure of the activate iron species in the montmorillonite was an amorphous FeO(OH)-like structure after calcining at 500 °C. The obtained catalysts showed high photo-Fenton activities in both degradation and mineralization of phenol solution. Due to larger surface area and more active iron species, the as-prepared Fenton catalysts showed much higher activity than the traditional iron hydroxyl intercalated montmorillonite catalyst. This catalyst was stable and could keep the high photo-Fenton performance during the long-operation process, implying that it had great potential application for the treatment of agro-industrial wastewater. This strategy is also expected to be extended to the preparation of new Fenton catalysts with better performance from larger iron cluster intercalated layers of supporters.

Acknowledgements

This research was supported by the National Natural Science Foundation of China (20777011), the National Key Basic Research Program of China (973 Program: 2007CB613306) and the program for Changjiang scholars and Innovative Research Team in University (PCSIRT0818). We also thank for the help of SSRF (Shanghai Synchrotron Radiation Facility) in the characterization of the XAFS.

References

[1] M. Noorjahan, V. Durga Kumari, M. Subrahmanyam, L. Panda, Appl. Catal. B: Environ. 57 (2005) 291–298.
[2] R. Savidha, A. Pandurangan, M. Palaichamy, V. Murugesan, Catal. Lett. 91 (2003) 1–2.
[3] M.M. Cheng, W.H. Ma, J. Li, Y.P. Huang, J.C. Zhao, Environ. Sci. Technol. 38 (2004) 1569–1575.
[4] M.A. De León, J. Castiglioni, J. Bussi, M. Sergio, Catal. Today 133–135 (2008) 600–605.
[5] J. Gao, L. Wu, S.J. Liang, S.L. Zhang, P. Liu, X.Z. Fu, Chin. J. Catal. 31 (2010) 317–321.
[6] J. Fernandez, J. Bandara, A. Lopez, Ph. Buffar, J. KiWi, Langmuir 15 (1999) 185–192.
[7] S.G. Hur, T.W. Kim, S.J. Hwang, S.H. Huang, J.H. Yang, J.H. Choy, J. Phys. Chem. B 110 (2006) 1599–1604.
[8] M.L. Schlegel, A. Manceau, Environ. Sci. Technol. 41 (2007) 1942–1948.
[9] T. Polubesova, Y. Chen, R. Navon, B. Chefetz, Environ. Sci. Technol. 42 (2008) 4797–4803.
[10] J.H. Choy, H. Jung, Y.S. Han, J.B. Yoon, Y.G. Shul, H.J. Kim, Chem. Mater. 14 (2002) 3823–3828.
[11] L.Z. Zhu, B.L. Chen, X.Y. Shen, Environ. Sci. Technol. 34 (2000) 468–475.
[12] S.A. Boyd, J.F. Lee, M.M. Mortland, Nature 333 (1988) 345–347.

[13] J.A. Smith, A. Galan, Environ. Sci. Technol. 29 (1995) 685–692.
[14] C. Catrinescu, C. Teodosiu, M. Macoveanu, J. Miehe-Brendlé, R. Le Dred, Water Res. 37 (2003) 1154–1160.
[15] J.Y. Feng, X.J. Hu, P.L. Yue, Environ. Sci. Technol. 38 (2004) 269–275.
[16] J.Y. Feng, X.J. Hu, P.L. Yue, Environ. Sci. Technol. 38 (2004) 5773–5778.
[17] T. Mishra, K.M. Parida, S.B. Rao, J. Colloid Interface Sci. 183 (1996) 176–183.
[18] J.X. Chen, L.Z. Zhu, Catal. Today 126 (2007) 463–470.
[19] S.W. Lam, K. Chiang, T.M. Lim, R. Amal, G.K.-C. Low, J. Catal. 234 (2005) 292–299.
[20] Y.H. Son, J.K. Lee, Y. Soong, D. Martello, M. Chyu, Chem. Mater. 22 (2010) 2226–2232.
[21] M.J.P. Zurita, G. Vitale, M.R. de Goldwasser, J. Mol. Catal. A: Chem. 107 (1996) 175–183.
[22] R. Issaadi, F. Garin, C.E. Chitour, G. Maire, Appl. Catal. A 207 (2001) 323–332.
[23] S. Yamanaka, T. Sako, M. Hauori, Mater. Res. Bull. 19 (1984) 161.
[24] G.B. Ortiz de la Plata, O.M. Alfano, A.E. Cassano, Appl. Catal. B: Environ. 95 (2010) 1–13.
[25] H. Xie, Y.Z. Li, S.F. Jin, J.J. Han, X.J. Zhao, J. Phys. Chem. C 114 (2010) 9706–9712.
[26] J.B. Zhang, J. Zhuang, L.Z. Gao, Y. Zhang, N. Gu, J. Feng, D.L. Yang, J.D. Zhu, X.Y. Yan, Chemosphere 73 (2008) 1524–1528.
[27] J. de Laat, H. Gallard, Environ. Sci. Technol. 33 (1999) 2726–2732.
[28] D.W. Park, B.G. Kim, M.I. Kim, I. Kim, H.C. Woo, Catal. Today 93–95 (2004) 235–240.
[29] F. Heinrich, C. Schmidt, E. Löffler, M. Menzel, W. Grünert, J. Catal. 212 (2002) 157–172.
[30] Y. Wang, Q. Zhang, T. Shishido, K.J. Takehira, J. Catal. 209 (2002) 186.
[31] G.Y. Yan, J.L. LoNG, X.X. Wang, Z.H. Li, X.C. Wang, Y.M. Xu, X.Z. Fu, J. Phys. Chem. C 111 (2007) 5195–5202.
[32] M. Schwidder, M.S. Kumar, K. Klementiev, M.M. Pohl, A. Brückner, W. Grünert, J. Catal. 231 (2005) 314.
[33] H.G. Yu, H. Irie, Y. Shimodaira, Y. Hosogi, Y. Kuroda, M. Miyauchi, K. Hashimoto, J. Phys. Chem. 114 (2010) 16481–16487.
[34] H. Irie, S. Miura, K. Kamiya, K. Hashimoto, Chem. Phys. Lett. 457 (2008) 202.
[35] F. Mijangos, F. Varona, N. Villota, Environ. Sci. Technol. 40 (2006) 5538–5543.
[36] S. Esplugas, J. Giménez, S. Contreras, E. Pascual, M. Rodríguez, Water Res. 36 (2002) 1034–1042.
[37] J.G. Yu, X.X. Yu, B.B. Huang, X.Y. Zhang, Y. Dai, Cryst. Growth Des. 9 (2009) 1474–1480.